

Adiabatic hyperspherical study of triatomic helium systems

Hiroya Suno

Japan Agency for Marine-Earth Science and Technology (JAMSTEC),

3173-25 Showa-machi, Kanazawa-ku, Yokohama 236-0001, Japan

B.D. Esry

Department of Physics, Kansas State University, Manhattan, Kansas 66506, USA

(Dated: November 11, 2019)

Abstract

The ${}^4\text{He}_3$ system is studied using the adiabatic hyperspherical representation. We adopt the current state-of-the-art helium interaction potential including retardation and the nonadditive three-body term, to calculate all low-energy properties of the triatomic ${}^4\text{He}$ system. The bound state energies of the ${}^4\text{He}$ trimer are computed as well as the ${}^4\text{He}+{}^4\text{He}_2$ elastic scattering cross sections, the three-body recombination and collision induced dissociation rates at finite temperatures. We also treat the system that consists of two ${}^4\text{He}$ and one ${}^3\text{He}$ atoms, and compute the spectrum of the isotopic trimer ${}^4\text{He}_2 {}^3\text{He}$, the ${}^3\text{He}+{}^4\text{He}_2$ elastic scattering cross sections, the rates for three-body recombination and the collision induced dissociation rate at finite temperatures. The effects of retardation and the nonadditive three-body term are investigated. Retardation is found to be significant in some cases, while the three-body term plays only a minor role for these systems.

I. INTRODUCTION

Three-body atomic systems have attracted considerable interest due to the possibility of observing an intriguing property generally referred to as "Efimov physics" [1, 2, 3]. The most dramatic manifestation of Efimov physics is the possibility of an infinity of three-body bound states even when none exist for the separate two-body subsystems. This occurs when the two-body scattering length a_{12} is large compared to the characteristic range r_0 of the two-body interaction potential, which is typically on the order of tens of Bohr radii. It is predicted that, in the limit of large scattering length (therefore zero two-body binding energy), the atom-dimer scattering length also becomes large and the three-body system acquires an infinite series of bound states (called Efimov states) whose energies form a geometric sequence with zero as an accumulation point. These phenomena persist even when r_0/a_{12} is nonzero, so that we can expect to observe Efimov physics in a real physical system. The theory of Efimov physics was formulated in 1970 [1, 2, 3], but was experimentally confirmed only in 2006 [4], by exploiting a Feshbach resonance in an ultracold gas of ^{133}Cs atoms to adjust the scattering length. However, the evidence of Efimov physics was seen in the three-body recombination rates, not by direct observation of bound states. It is therefore clear that understanding three-body recombination is crucial in establishing the extent to which Efimov physics can be realized in the laboratory.

Helium has long been considered to be one of the most promising candidates for seeing Efimov physics since the ^4He dimer has a large scattering length (larger than 100 a.u.). The theoretical treatment of triatomic ^4He systems is simple compared to other atomic species because there exists only one dimer bound state which has zero orbital angular momentum $l = 0$. Several sophisticated helium dimer interaction potentials have been developed, of which the most widely used one is probably the LM2M2 potential by Aziz and Slaman [5]. This potential has been used to calculate various properties of the helium dimer and trimer [6, 7, 8, 9] as well as their scattering observables [10, 11, 12, 13]. The HFD-B3-FCI1 potential developed by Aziz *et al.* [14] has also been used to calculate the three-body recombination rates of cold helium atoms [15, 16, 17]. Jeziorska *et al.* [18] and Cencek *et al.* [19] have recently developed not only a helium dimer potential, but also the retardation correction to the dimer potential and the nonadditive three-body term. Retarded potentials have been used previously [13, 20] and were found to have clear impacts on the low-energy

behavior of helium systems. Experimentally, the ^4He dimer has been observed by Luo *et al.* [21, 22] and by Schöllkopf and Toennies [23, 24]. The latter authors were able to see not only the helium dimer but also the trimer and tetramer. The ^4He trimer they observed was in its ground state, but no experiment has been able to see the excited state. There is actually much discussion currently whether one or both of these states should be considered Efimov states.

This work is along the line of the investigations in Refs. [6, 7, 8, 9, 10, 11, 12, 13, 15, 16, 17, 25, 26], which dealt with the spectrum of the helium trimer, the atom-dimer elastic scattering in triatomic helium systems, and the three-body recombination of cold helium atoms. None of these previous works, however, presented all of these quantities. By doing so, we hope to benefit those applying effective field theory to this system. Moreover, we adopt the current state-of-the-art triatomic helium interaction potential, including the two-body term with retardation by Jeziorska *et al.* [18, 27] and the nonadditive three-body term of Cencek *et al.* [19]. Using this complete potential, we compute the bound state energies of the ^4He trimer and the cross sections for elastic scattering between ^4He and $^4\text{He}_2$. We also calculate the rates for three-body recombination $^4\text{He}+^4\text{He}+^4\text{He}\rightarrow^4\text{He}_2+^4\text{He}$ and collision induced dissociation $^4\text{He}_2+^4\text{He}\rightarrow^4\text{He}+^4\text{He}+^4\text{He}$ at finite temperatures. In our previous paper [15], we published the recombination and dissociation rates using the HFD-B3-FCI1 potential and including the states with total angular momenta from $J = 0$ to 3. In the present work, we extend the calculations up to $J = 7$ using the new potential mentioned above. In addition, we treat the system consisting of two ^4He and one ^3He atoms, and calculate both its spectrum and the cross sections for elastic scattering between $^4\text{He}_2$ and ^3He . We also obtain the rates for three-body recombination $^4\text{He}+^4\text{He}+^3\text{He}\rightarrow^4\text{He}_2+^3\text{He}$ and collision induced dissociation $^4\text{He}_2+^3\text{He}\rightarrow^4\text{He}+^4\text{He}+^3\text{He}$ at finite temperatures for the first time. To summarize, we will present calculations of all low-energy properties of triatomic helium for the isotopic combinations that include $^4\text{He}_2$. Moreover, we do so using the best available potentials and examine the contribution of the usually-neglected retardation and purely three-body terms.

The key ingredient in our numerical calculations is the adiabatic hyperspherical representation [6, 15, 28]. Enforcing the boson permutation symmetry is simplified using a modified version of the Smith-Whitten coordinate system [15, 29, 30]. The R -matrix method [31] is used to obtain the scattering S -matrix. Using this S -matrix, we calculate the atom-dimer

elastic scattering cross sections σ_2 , as well as the rates for three-body recombination K_3 and collision induced dissociation D_3 . Note that the rate equation for the density of helium atoms in a thermal gas can be written as

$$\frac{dn_4}{dt} = -\frac{2}{3!}K_3n_4^3 - \frac{2}{2!}K'_3n_4^2n_3 + 2D_3n_{4d}n_4 + 2D'_3n_{4d}n_3, \quad (1)$$

where n_4 , n_{4d} and n_3 are the densities of ${}^4\text{He}$, ${}^4\text{He}_2$ and ${}^3\text{He}$, respectively. K_3 and K'_3 are the rates for the recombination processes ${}^4\text{He}+{}^4\text{He}+{}^4\text{He}\rightarrow{}^4\text{He}_2+{}^4\text{He}$ and ${}^4\text{He}+{}^4\text{He}+{}^3\text{He}\rightarrow{}^4\text{He}_2+{}^3\text{He}$, respectively, while D_3 and D'_3 are the rates for the dissociation processes ${}^4\text{He}_2+{}^4\text{He}\rightarrow{}^4\text{He}+{}^4\text{He}+{}^4\text{He}$ and ${}^4\text{He}_2+{}^3\text{He}\rightarrow{}^4\text{He}+{}^4\text{He}+{}^3\text{He}$, respectively.

This paper is organized as follows. We explain our method and give all necessary formulas for calculating the spectra and the collision properties of triatomic helium systems in Sec. II. The results are presented in Sec. III. A summary of this work is given in Sec. IV. We use atomic units throughout except where explicitly stated otherwise.

II. METHOD

We solve the Schrödinger equation for three interacting helium atoms using the adiabatic hyperspherical representation [6, 15, 28]. In the adiabatic hyperspherical representation, we calculate eigenfunctions and eigenvalues of the fixed-hyperradius Hamiltonian in order to construct a set of coupled radial equations. The bound state energies can be obtained as the discrete eigenvalues of these coupled equations. The scattering S -matrix can be extracted from the same coupled equations using the R -matrix method. The method employed is largely the same as detailed in Ref. [15]. We thus give here a brief outline, emphasizing the modifications necessary when the three particles are not identical.

After separation of the center of mass motion, any three-particle system (in the absence of an external field) can be described by six coordinates. Three of these can be chosen as the Euler angles α , β , and γ that specify the orientation of the body-fixed frame relative to the space-fixed frame. The remaining three internal coordinates can be represented by a hyperradius R and two hyperangles θ and φ . To define these internal coordinates, we use a slightly modified version of the Smith-Whitten hyperspherical coordinates [15, 29, 30, 32, 33]. We first introduce the three-body reduced mass μ and the scale parameters d_{ij} as follows:

$$\mu^2 = \frac{m_1m_2m_3}{m_1 + m_2 + m_3}, \quad (2)$$

$$d_{ij}^2 = \frac{(m_k/\mu)(m_i + m_j)}{m_i + m_j + m_k}, \quad (3)$$

where the indices i, j, k are a cyclic permutation of $(1, 2, 3)$. The mass-scaled Jacobi coordinates [34, 35] are defined by

$$\vec{\rho}_1 = (\vec{r}_2 - \vec{r}_1)/d_{12}, \quad (4)$$

$$\vec{\rho}_2 = d_{12} \left[\vec{r}_3 - \frac{m_1 \vec{r}_1 + m_2 \vec{r}_2}{m_1 + m_2} \right]. \quad (5)$$

Here, \vec{r}_i is the position of the particle i with mass m_i in the lab-fixed frame. We shall write the hyperradius R as follows:

$$R^2 = \rho_1^2 + \rho_2^2, \quad R \in [0, \infty). \quad (6)$$

The hyperangles θ and φ are defined by

$$\begin{aligned} (\vec{\rho}_1)_x &= R \cos(\pi/4 - \theta/2) \cos(\varphi/2 + \varphi_{12}/2), \\ (\vec{\rho}_1)_y &= R \sin(\pi/4 - \theta/2) \sin(\varphi/2 + \varphi_{12}/2), \\ (\vec{\rho}_1)_z &= 0, \\ (\vec{\rho}_2)_x &= -R \cos(\pi/4 - \theta/2) \sin(\varphi/2 + \varphi_{12}/2), \\ (\vec{\rho}_2)_y &= R \sin(\pi/4 - \theta/2) \cos(\varphi/2 + \varphi_{12}/2), \\ (\vec{\rho}_2)_z &= 0, \end{aligned} \quad (7)$$

where $\varphi_{12} = 2 \arctan(m_2/\mu)$. In the case of three identical particles, the hyperangle φ can be reduced from $[0, 2\pi]$ to $[0, 2\pi/3]$ in which case the interaction potential becomes invariant under reflections about $\varphi = \pi/3$. Then, in this restricted domain, the solutions of the Schrödinger equation are automatically either symmetric (bosonic) or antisymmetric (fermionic) with respect to exchange of any two particles (this assumes the spin wave function is completely symmetric under exchange of any two particles). In the case that two of the three particles (we choose particles 2 and 3) are identical, the interaction potential becomes invariant under reflections about $\varphi = \pi$, and the solutions of the Schrödinger equation are automatically either symmetric (bosonic) or antisymmetric (fermionic) in the range $[0, 2\pi]$ with respect to exchange of the particles 2 and 3. Note that the definition of the hyperangle φ in Eqs. (7) is slightly different from that of $\varphi^{\text{prev.}}$ in our previous publication [15]. The relationship between the present and previous definitions is given by $\varphi = \varphi^{\text{prev.}} - 4\pi/3$. To demonstrate the effect of particle permutations on the hyperangle φ , Fig. 1 shows contour

plots of the potential energy surfaces for both three identical particles and two identical particles.

In our hyperspherical coordinates, the interparticle distances are given by

$$\begin{aligned} r_{12} &= 2^{-1/2}d_{12}R[1 + \sin\theta \cos(\varphi + \varphi_{12})]^{1/2}, \\ r_{23} &= 2^{-1/2}d_{23}R[1 + \sin\theta \cos\varphi]^{1/2}, \\ r_{31} &= 2^{-1/2}d_{31}R[1 + \sin\theta \cos(\varphi + \varphi_{31})]^{1/2}, \end{aligned} \quad (8)$$

with

$$\varphi_{12} = 2 \arctan(m_2/\mu), \quad \varphi_{31} = -\arctan(m_3/\mu). \quad (9)$$

We rewrite the Schrödinger equation in terms of a rescaled wavefunction, which is related to the usual Schrödinger solution Ψ by $\psi = R^{5/2}\Psi$. The volume element relevant to integrals over $|\psi|^2$ then becomes $2dR \sin 2\theta d\theta d\varphi d\alpha \sin \beta d\beta d\gamma$. The Schrödinger equation for three particles interacting through $V(R, \theta, \varphi)$ now takes the form

$$\left[-\frac{1}{2\mu} \frac{\partial^2}{\partial R^2} + \frac{\Lambda^2}{2\mu R^2} + \frac{15}{8\mu R^2} + V(R, \theta, \varphi) \right] \psi = E\psi, \quad (10)$$

where Λ^2 is the squared “grand angular momentum operator” and its expression is given in Refs. [15, 30, 33].

The interaction potential $V(R, \theta, \varphi)$ used in this work is expressed as a sum of three two-body terms and a nonadditive three-body term:

$$V(R, \theta, \varphi) = v(r_{12}) + v(r_{23}) + v(r_{31}) + w(r_{12}, r_{23}, r_{31}). \quad (11)$$

For the helium dimer potential $v(r)$, we use the representation of Jeziorska *et al.*, given in Ref. [18]. The retardation effect can be incorporated as an additional correction term [27] to the dimer potential. Due to this correction, the usual van der Waals term $C_6 r^{-6}$, valid at short range, transforms into $C_7 r^{-7}$ at long range. The $^4\text{He}_2$ bound state energies $E_{vl} = E_{00}$ and scattering lengths a_{12} calculated with the retarded and unretarded dimer potentials are summarized in Table I and reproduce those found in Ref. [18]. For comparison, the dimer energy with the older LM2M2 potential is -130 mK [6], giving a scattering length of 100\AA [12]. Comparison with other available potentials shows general agreement in that all give a weakly bound dimer, but the energy can vary by a factor of two [12, 20]. There is every reason to believe, however, that the current potential is the best available (see discussion in Ref. [18]). No bound state exists for $^4\text{He}^3\text{He}$ or $^3\text{He}_2$.

For the nonadditive three-body term $w(r_{12}, r_{23}, r_{31})$, Cencek *et al.* [19] give two representations. One is based on symmetry-adapted perturbation theory (SAPT); the other, on supermolecular coupled-cluster theory with single, double and noniterative triple excitations [CCSD(T)]. As mentioned in Ref. [19], these two representations are very close to each other. In test calculations, we find that the three-body problem shows no noticeable difference between the SAPT and CCSD(T) representations, and the numerical results agree with each other to four significant digits. Consequently, the results we present here will use only the SAPT representation of the three-body term. In the remainder of this paper, we will use the term "complete interaction" to indicate that retardation and the three-body term have been included.

The first step that must be carried out is the solution of the fixed- R adiabatic eigenvalue equation for a given symmetry J^Π , with Π the total parity, to determine the adiabatic eigenfunctions (or channel functions) and eigenvalues (or potential curves). The adiabatic eigenfunction expansion gives the wavefunction $\psi(R, \Omega)$ [we will write $\Omega \equiv (\theta, \varphi, \alpha, \beta, \gamma)$] in terms of the complete, orthonormal set of angular wavefunctions Φ_ν and radial wavefunctions F_ν

$$\psi(R, \Omega) = \sum_{\nu=0}^{\infty} F_\nu(R) \Phi_\nu(R; \Omega). \quad (12)$$

The channel functions Φ_ν are eigenfunctions of the five-dimensional partial differential equation

$$\left[\frac{\Lambda^2}{2\mu R^2} + \frac{15}{8\mu R^2} + V(R, \theta, \varphi) \right] \Phi_\nu(R; \Omega) = U_\nu(R) \Phi_\nu(R; \Omega), \quad (13)$$

whose solutions depend parametrically on R . Insertion of ψ from Eq. (12) into the Schrödinger equation from Eq. (10) results in a set of coupled ordinary differential equations

$$\begin{aligned} & \left[-\frac{1}{2\mu} \frac{d^2}{dR^2} + U_\nu(R) - \frac{1}{2\mu} Q_{\nu\nu}(R) \right] F_\nu(R) \\ & - \frac{1}{2\mu} \sum_{\nu' \neq \nu} \left[2P_{\nu\nu'}(R) \frac{d}{dR} + Q_{\nu\nu'}(R) \right] F_{\nu'}(R) = E F_\nu(R). \end{aligned} \quad (14)$$

The coupling elements $P_{\nu\nu'}(R)$ and $Q_{\nu\nu'}(R)$ involve partial first and second derivatives of the channel functions Φ_ν with respect to R , and are defined as follows

$$P_{\nu\nu'}(R) = \left\langle\left\langle \Phi_\nu(R; \Omega) \left| \frac{\partial}{\partial R} \right| \Phi_{\nu'}(R; \Omega) \right\rangle\right\rangle, \quad (15)$$

and

$$Q_{\nu\nu'}(R) = \left\langle\left\langle \Phi_\nu(R; \Omega) \left| \frac{\partial^2}{\partial R^2} \right| \Phi_{\nu'}(R; \Omega) \right\rangle\right\rangle. \quad (16)$$

The double-bracket matrix element signifies that integrations are carried out only over the angular coordinates Ω .

When solving the adiabatic equation (13), the degrees of freedom corresponding to the Euler angles α , β and γ are treated by expanding the channel functions $\Phi_\nu(R; \Omega)$ on Wigner D functions [15]. The remaining degrees of freedom θ and φ are dealt with by expanding the channel function onto a direct product of fifth order basis splines [36]. We generate the basis splines for θ from 100 mesh points, while we use 80 mesh points for φ . For small hyperradii R , a uniform mesh is employed; for large R , the mesh is designed so that it become dense around the two-body coalescence points at $(\theta, \varphi) = (\pi/2, \pi - \varphi_{12})$, $(\pi/2, \pi)$ and $(\pi/2, \pi - \varphi_{31})$, where the potential surface $V(R, \theta, \varphi)$ changes abruptly. This leads, for example, to a total basis size of 34528 in the case of the 3^- symmetry. We autoparallelize the computer program in order to run it on multiple CPU cores. Typically, a calculation of the 32 lowest eigenvalues of the adiabatic equation (13) takes about 5 minutes of wall clock time using 8 1.6-GHz-Itanium2 CPU cores on an SGI Altix 4700 supercomputer. We note that our approach, unlike many others employed for this problem, does not use a partial wave expansion in the Jacobi-coordinate angular momenta. Our results are, in fact, equivalent to including a large number of such partial waves.

The identical particle symmetry was built into the adiabatic equations via the boundary conditions in φ . For details, see Ref. [15]. For the case of three identical particles, we have

$$\Phi_\nu(R; \theta, \varphi = 0, \alpha, \beta, \gamma) = \pm \Phi_\nu(R; \theta, \varphi = \frac{2\pi}{3}, \alpha, \beta, \gamma), \quad \text{for } \Pi = \pm 1, \quad (17)$$

and for the case of two identical particles

$$\Phi_\nu(R; \theta, \varphi = 0, \alpha, \beta, \gamma) = \pm \Phi_\nu(R; \theta, \varphi = 2\pi, \alpha, \beta, \gamma), \quad \text{for } \Pi = \pm 1. \quad (18)$$

These conditions ensure that each solution is either symmetric or antisymmetric with respect to exchange of any two identical particles (about half of the solutions are symmetric), thus eliminating all states of mixed symmetry. The channel functions with appropriate exchange symmetry are then extracted in a postsymmetrization procedure as the solutions that satisfy

$$\left\langle\left\langle \Phi_\nu(R; \Omega) \left| \frac{1 + P_{12}}{2} \right| \Phi_\nu(R; \Omega) \right\rangle\right\rangle = 1 \quad (19)$$

for the case of three identical bosons, and

$$\left\langle\left\langle \Phi_\nu(R; \Omega) \left| \frac{1 + P_{23}}{2} \right| \Phi_\nu(R; \Omega) \right\rangle\right\rangle = 1 \quad (20)$$

for the case of two identical bosons.

In practice we solve the adiabatic equation (13) for a set of about 200 radial grid points R_i up to $R \approx 2000$ a.u. in order to obtain the potential curves $U_\nu(R)$ and the coupling matrix elements $P_{\nu\nu'}(R)$ and $Q_{\nu\nu'}(R)$. For $R > 2000$ a.u. they are extrapolated using their known asymptotic forms. The details of the numerical calculations are explained in Ref. [15].

III. RESULTS AND DISCUSSION

As predicted by several authors [6, 7, 8, 9, 12, 13, 20, 25, 26, 37, 38], bound states for ${}^4\text{He}_3$ and ${}^4\text{He}_2 {}^3\text{He}$ can exist only for $J^\Pi = 0^+$, and none for $J > 0$. Since the ${}^4\text{He}$ dimer has only a single $l = 0$ bound state, atom-dimer scattering, three-body recombination and collision induced dissociation are allowed only for the parity-favored cases, that is, $\Pi = (-1)^J$. In the following, we therefore limit ourselves to $J^\Pi = 0^+, 1^-, 2^+$, etc... For each of these cases, the lowest adiabatic potential curve $\nu = 0$ corresponds asymptotically to two atoms bound in a dimer with the third atom far away. Since the dimer has only $l = 0$, the orbital angular momentum of the relative motion between the dimer and the atom should be $l_{1,23} = J$. This potential asymptotically behaves as

$$U_0(R) - \frac{1}{2\mu}Q_{00}(R) \rightarrow E_{00} + \frac{l_{1,23}(l_{1,23} + 1)}{2\mu R^2}, \quad \text{for } R \rightarrow \infty, \quad (21)$$

where E_{00} is the energy of ${}^4\text{He}_2$. All the higher channels $\nu = 1, 2, 3, \dots$ for each symmetry correspond to three-body continuum states i.e., all three atoms far away from each other as $R \rightarrow \infty$. Recall that in the adiabatic hyperspherical representation the three-body continuum is rigorously discretized since the adiabatic Hamiltonian depends only on the bounded hyperangles. These three-body continuum channel functions converge asymptotically to the hyperspherical harmonics. Therefore, the corresponding potential curves behave as

$$U_\nu(R) \rightarrow \frac{\lambda(\lambda + 4) + \frac{15}{4}}{2\mu R^2}, \quad \text{for } R \rightarrow \infty. \quad (22)$$

In principle, λ can take on any non-negative integer value, but their possible values are restricted by the requirements of permutation symmetry. Figure 2 shows the potential curves $U_\nu(R)$ as functions of the hyperradius R for ${}^4\text{He}_3$ and ${}^4\text{He}_2 {}^3\text{He}$, $J^\Pi = 0^+$. Note that we have also calculated potential curves for ${}^4\text{He}_3$ system with $J^\Pi = 1^-, \dots, 7^-$, and for ${}^4\text{He}_2 {}^3\text{He}$ with $J^\Pi = 1^-, 2^+$ and 3^- .

Although we will present cross sections and rates as a function of temperature, they are not thermally averaged. Rather, the temperature is obtained from the energy by the conversion noted in Table I. If needed, the thermal average can be carried out as described in Ref. [39] for K_3 or as described in Ref. [40] for two-body processes.

A. Bound state energies

The bound state energies can be obtained as the discrete eigenenergies of the coupled equations in Eq. (14). We solve these equations by expanding $F_\nu(R)$ onto a set of fifth order basis splines in R . Typically, a solution of the coupled equations including 10 adiabatic channels takes about 1 minute of CPU time using one 1.6-GHz-Itanium2 processor on an SGI Altix 4700 supercomputer.

The "adiabatic approximation" is the solution of Eq. (14) with only one channel ν , which eliminates the sum over ν' on the left-hand side of the equation. This leaves a one-dimensional Schrödinger equation with an effective hyperradial potential $U_\nu(R) - \frac{1}{2\mu}Q_{\nu\nu}(R)$ that determines the three-body spectrum in the adiabatic approximation. The lowest $\nu = 0$ energy level obtained by solving Eq. (14) with all nondiagonal coupling elements neglected is a variational upper bound to the true ground state energy E_0 . One can also solve Eq. (14) neglecting the diagonal coupling term $Q_{\nu\nu}(R)$. This corresponds to the hyperspherical equivalent of the Born-Oppenheimer approximation. The lowest resulting energy for $\nu = 0$ gives a rigorous lower bound to E_0 . Finally, solving Eq. (14) with the sums truncated at ν_{\max} gives variational approximations to the exact energies. These energies will thus converge to the exact energies from above in the limit $\nu_{\max} \rightarrow \infty$.

As in previous investigations [6, 7, 8, 9, 12, 13, 20, 25, 26, 37, 38], we find two bound states for $^4\text{He}_3$ and one for $^4\text{He}_2\ ^3\text{He}$. Table II summarizes these different levels of approximation to the bound state energies of $^4\text{He}_3$ and $^4\text{He}_2\ ^3\text{He}$ as well as the convergence with respect to ν_{\max} . We also include an estimate of the exact energy obtained by extrapolating the ν_{\max} -dependent energies using $E_{\nu_{\max}} = E_{\text{exact}} + \alpha/\nu_{\max}^\beta$. The relatively slow convergence in the number of channels is due, we think, to the large repulsive core of the helium interaction potential. To conclude, we have obtained $E_0 = -130.86$ mK and $E_1 = -2.5882$ mK for $^4\text{He}_3$ and $E_0 = -16.237$ mK for $^4\text{He}_2\ ^3\text{He}$ with the complete interaction potential. For comparisons, Nielsen *et al.* [8] obtained $E_0 = -125.2$ mK and $E_1 = -2.269$ mK for $^4\text{He}_3$

and $E_0 = -13.66$ mK for ${}^4\text{He}_2 {}^3\text{He}$, using the LM2M2 potential. Using the same LM2M2 potential, Blume *et al.* [7] obtained $E_0 = -125$ mK and $E_1 = -2.28$ mK for ${}^4\text{He}_3$. Moreover, these energies are also in general agreement with those obtained for other two-body potentials.

From the table, it can be seen that more than 30 channels are needed to obtain convergence to four digits and that ${}^4\text{He}_3$ converges more quickly than ${}^4\text{He}_2 {}^3\text{He}$. It is also clear that the adiabatic approximation is better than the Born-Oppenheimer as has been noted before [6, 7]. Table II also shows the effects of retardation and the three-body terms. Comparing the converged results, we see that the complete potential reduces the binding compared to the simple pairwise, unretarded potential. In all cases, retardation is more important than the three-body term, giving roughly an order of magnitude larger shift in the bound state energies. Given the relative importance of retardation, it is clear why the energies are shifted upwards since the retardation corrections shortens the tail of the potentials from r^{-6} to r^{-7} . Physically, it is also easy to understand why the three-body term is relatively unimportant once one notes that its leading-order contribution is the Axilrod-Teller, dipole-dipole-dipole dispersion term. Because helium is closed shell and tightly bound, its polarizability is small, yielding small dispersion terms in general. We conclude, then, that the relative importance of retardation and the three-body term found here should not be assumed to be a general result.

B. Atom-dimer elastic scattering cross sections

The scattering observables were obtained by solving the coupled equations (14) using a combination of the finite element method (FEM) [40] and the R -matrix method [31]. Typically, about 12 adiabatic channels (thus $\nu_{\text{max}} = 11$) are used, and 10^4 elements, in each of which fifth order polynomials are used to expand the radial wavefunction, extend from $R = 5$ to 5×10^5 a.u. The scattering S -matrix is then extracted using the R -matrix method. Each energy took less than 1 minute of wall clock time using one 1.6 GHz Itanium2 processor on an SGI Altix 4700 supercomputer. We have checked the stability of the S -matrix with respect to the final matching distance, number of FEM sectors, and the number of coupled channels, and have found our results accurate to two significant digits.

The cross section for atom-dimer elastic scattering is expressed in terms of the S -matrix

as

$$\sigma_2 = \sum_{J,\Pi} \sigma_2^{J\Pi} = \sum_{J,\Pi} \frac{(2J+1)\pi}{k_{1,23}^2} |S_{0\leftarrow 0}^{J\Pi} - 1|^2. \quad (23)$$

Here, $\sigma_2^{J\Pi}$ is the partial atom-dimer elastic scattering cross section corresponding to the $J\Pi$ symmetry, $k_{1,23} = [2\mu_{1,23}(E - E_{00})]^{1/2}$ is the atom-dimer wavenumber and $\mu_{1,23}$ is the atom-dimer reduced mass $\mu_{1,23} = m_1(m_2 + m_3)/(m_1 + m_2 + m_3)$. The event rate constant K_2 is related to the cross section by the formula $K_2 = k_{1,23}\sigma_2/\mu_{1,23}$.

The atom-dimer scattering length is another useful quantity that has been studied [9, 11, 12, 13, 16, 26]. It is defined as

$$a_{1,23} = - \lim_{k_{12,3} \rightarrow 0} \frac{\tan \delta_0}{k_{1,23}}, \quad (24)$$

where δ_0 is the phase-shift for atom-dimer elastic scattering and is related to the diagonal S -matrix element by the formula

$$S_{0\leftarrow 0}^{0+} = \exp(2i\delta_0). \quad (25)$$

Figure 3(a) presents the partial cross sections $\sigma_2^{J\Pi}$ for elastic ${}^4\text{He}+{}^4\text{He}_2$ scattering as functions of the collision energy $(E - E_{00})$ for the $J\Pi = 0^+, 1^-, \dots, 7^-$ symmetries. The results obtained with the complete helium interaction potential are shown. For comparisons, the figure also shows calculations with various combinations of retarded two-body potential and three-body term for the $J\Pi = 0^+$ and 2^+ symmetries. In the ultracold limit, here $E - E_{00} < 30\mu\text{K}$, σ_2^{0+} is constant and tends towards the value $\sigma_2^{0+} \rightarrow 4\pi a_{1,23}^2$, with $a_{1,23} = 230 \text{ a.u.} = 120\text{\AA}$. For comparison, Motovilov *et al.* [12] obtained $a_{1,23} = 115.5\text{\AA}$, using the LM2M2 potential. Curiously, the $J > 0$ partial cross sections decrease as functions of the energy for low energy, behaving as $\sigma_2^{J\Pi} \propto (E - E_{00})^{-1}$. From the Wigner threshold law, however, one would expect them to behave as $\sigma_2^{J\Pi} \propto (E - E_{00})^J$, since J is the orbital angular momentum of the atom relative to the dimer. We have found, though, that collision energies of some μK are still too large to recover this threshold behavior and that the cross sections reach the threshold regime only at collision energies less than about 1 nK. The effects of retardation and the three-body term are almost negligible for $J\Pi = 0^+$, but for $J\Pi = 2^+$, retardation increases the partial cross section by about 75% for $E - E_{00} < 10^{-2} \text{ mK}$, while the three-body term has a smaller effect. The trend is reversed at collision energies higher than about 0.3 mK.

In Fig. 3(b) we present $\sigma_2^{J\Pi}$ for ${}^3\text{He}+{}^4\text{He}_2$ elastic scattering for the $J^\Pi = 0^+, 1^-, 2^+$ and 3^- symmetries. As in Fig. 3(a), we show the results obtained with the complete helium interaction potential and those calculated with all combinations of the retarded two-body potential and three-body term. For this system, we found $a_{1,23} = 40$ a.u.=21Å. For comparison, Sandhas *et al.* [13] obtained $a_{1,23} = 21.0\text{Å}$, using the LM2M2 potential. As found in the ${}^4\text{He}+{}^4\text{He}_2$ scattering, the collision energies are found to be still too large to show the Wigner threshold behavior $\sigma_2^{J\Pi} \propto (E - E_{00})^J$. The effects of retardation and the three-body term are almost negligible.

Figure 4 shows the phase shifts δ_0 for s -wave atom-dimer elastic scattering as functions of the collision energy. The lower curve shows the results for ${}^4\text{He}+{}^4\text{He}_2$; and the upper one, for ${}^3\text{He}+{}^4\text{He}_2$. These results were obtained from the complete potential, but we did not observe any visible difference from the results obtained neglecting the corrections on this scale.

C. Three-body recombination rates

With the S -matrix in hand, we can also calculate the three-body recombination rates. The event rate constant for three-body recombination for ${}^4\text{He}+{}^4\text{He}+{}^4\text{He}\rightarrow{}^4\text{He}_2+{}^4\text{He}$ is

$$K_3 = \frac{k}{\mu} \sigma_3^K = \sum_{J,\Pi} K_3^{J\Pi} = 3! \sum_{J,\Pi} \sum_{\nu=1}^{\nu_{\max}} \frac{32(2J+1)\pi^2}{\mu k^4} |S_{0\leftarrow\nu}^{J\Pi}|^2. \quad (26)$$

Here, $K_3^{J\Pi}$ is the partial recombination rate corresponding to the J^Π symmetry, and $k = (2\mu E)^{1/2}$ is the hyperradial wavenumber in the incident channel. $S_{0\leftarrow\nu}^{J\Pi}$ represents scattering from the initial three-body continuum channels ($\nu = 1, 2, \dots, \nu_{\max}$) to the final atom-dimer channel ($\nu = 0$) for the J^Π symmetry. The factor (3!) derives from the number of indistinguishable bosonic particles. In the same spirit, the rate for three-body recombination ${}^4\text{He}+{}^4\text{He}+{}^3\text{He}\rightarrow{}^4\text{He}_2+{}^3\text{He}$ is given by

$$K_3 = \frac{k}{\mu} \sigma_3^K = 2! \sum_{J,\Pi} \sum_{\nu=1}^{\nu_{\max}} \frac{32(2J+1)\pi^2}{\mu k^4} |S_{0\leftarrow\nu}^{J\Pi}|^2. \quad (27)$$

We have checked the stability of the results with respect to the final matching distance, number of FEM sectors, and the number of coupled channels. Typically, we found the results to be accurate to three significant digits at 100 mK.

Figure 5(a) shows the total rate K_3 for three-body recombination ${}^4\text{He}+{}^4\text{He}+{}^4\text{He}\rightarrow{}^4\text{He}_2+{}^4\text{He}$ as well as the partial rates $K_3^{J\Pi}$ for the $J^\Pi = 0^+, 1^-, 2^+, \dots, 7^-$

symmetries as functions of the collision energy E . The results obtained with the complete helium interaction potential are shown while the total rates calculated with the unretarded two-body potential and/or the nonadditive three-body term are also presented in the region $E < 1$ mK. At the lower collision energies, $K_3^{J^\Pi} \propto E^{\lambda_{\min}}$, where λ_{\min} is the minimum value of λ in Eq. (22) allowed by permutation symmetry. For $J^\Pi = 0^+, 1^-, 2^+$ and 3^- in ${}^4\text{He}_3$, we have $\lambda_{\min} = 0, 3, 2$ and 3 , respectively; for $J > 3$, $\lambda_{\min} = J$. These threshold behaviors are predicted by a generalized Wigner threshold law [41]. For collision energies $E < 30\mu\text{K}$, the total recombination rate K_3 is constant, and the 0^+ partial recombination rate $K_3^{0^+}$ dominates. In the ultracold limit, we obtain $K_3 = 9.93 \times 10^{-28}$ cm⁶/s with the complete helium interaction potential, while we have 4.45×10^{-28} cm⁶/s without retardation, 1.01×10^{-27} cm⁶/s without the three-body term, and 4.54×10^{-28} cm⁶/s without either correction. Hence, retardation increases the recombination rate by about 120%, while the three-body term has a much smaller effect, lowering the recombination rate by about 2%. The present results differ from our previous calculations [15] using the HFD-B3-FCI1 potential, which gave $K_3 = 7.1 \times 10^{-28}$ cm⁶/s. Shepard [16] also obtained $K_3 = 7.09 \times 10^{-28}$ cm⁶/s using the same potential.

Figure 5(b) shows the total rate K_3 for three-body recombination ${}^4\text{He}+{}^4\text{He}+{}^3\text{He} \rightarrow {}^4\text{He}_2+{}^3\text{He}$ as well as the partial rates $K_3^{J^\Pi}$ for the $J^\Pi = 0^+, 1^-, 2^+$ and 3^- symmetries as functions of the collision energy E . At the lower collision energies, $K_3^{J^\Pi} \propto E^{\lambda_{\min}}$, with $\lambda_{\min} = 0, 1, 2$ and 3 , for $J^\Pi = 0^+, 1^-, 2^+$ and 3^- , respectively [41]. In the ultracold limit, we obtain $K_3 = 9.83 \times 10^{-27}$ cm⁶/s with the complete helium interaction potential, while we have 8.97×10^{-27} cm⁶/s without retardation, 9.78×10^{-27} cm⁶/s without the three-body term, and 8.98×10^{-27} cm⁶/s without either correction. Hence, retardation increases the recombination rate by about 10%. We observe that the three-body term has a smaller effect by far than retardation, lowering the recombination rate by only about 0.05%. Interestingly, recombination is much more efficient here with K_3 an order of magnitude larger than the homonuclear case above.

D. Collision induced dissociation rates

We can easily calculate the rates for collision induced dissociation since they require the same S -matrix elements as recombination. The collision induced dissociation rate is

$$D_3 = \frac{k_{1,23}}{\mu_{1,23}} \sigma_3^D = \sum_{J,\Pi} D_3^{J\Pi} = \sum_{J,\Pi} \sum_{\nu=1}^{\nu_{\max}} \frac{(2J+1)\pi}{\mu_{1,23} k_{1,23}} |S_{\nu \leftarrow 0}^{J\Pi}|^2, \quad (28)$$

where $D_3^{J\Pi}$ is the partial dissociation rate corresponding to the J^Π symmetry.

Figure 6(a) shows D_3 for ${}^4\text{He}_2 + {}^4\text{He} \rightarrow {}^4\text{He} + {}^4\text{He} + {}^4\text{He}$ as well as the partial rates $D_3^{J\Pi}$ for $J^\Pi = 0^+, 1^-, 2^+, \dots, 7^-$. At the lower collision energies, $D_3^{J\Pi} \propto E^{\lambda_{\min}+2}$, with the same λ_{\min} as $K_3^{J\Pi}$ [41]. Because it uses exactly the same S -matrix elements as K_3 , the effects of retardation and the three-body term are similar. In particular, retardation increases D_3 by about 134% at low energies, but the three-body term has little effect, lowering the dissociation rate only by a few percent. In Fig. 6(b), we show D_3 for ${}^4\text{He}_2 + {}^3\text{He} \rightarrow {}^4\text{He} + {}^4\text{He} + {}^3\text{He}$.

IV. SUMMARY

In this work, we have carried out a study of triatomic helium systems using the adiabatic hyperspherical approach. Adopting the most realistic, state-of-the-art helium interaction potential available, we update and extend previous investigations on the bound state and scattering properties of the ${}^4\text{He}_3$ and ${}^4\text{He}_2 {}^3\text{He}$ systems. Based on the most accurate helium-helium interactions, these three-body potentials also include two-body retardation corrections as well as a non-additive three-body contribution. We have thus been able to confirm our statement in Ref. [15] that the three-body term plays only a minor role. In contrast, the effects of retardation are significant, increasing the three-body recombination rate by a factor of two to three.

Systems of ground-state helium atoms are relatively simple because there exists only one $l = 0$ dimer bound states for ${}^4\text{He}$. Further computational improvements must be implemented before we can extend this approach to the more complicated cases of alkali atoms, where the larger number of sharp nonadiabatic avoided crossings pose difficulties. Further, in alkali systems, we expect that the three-body term will play a much larger role as has been recognized previously [42, 43]. This work shows, however, that retardation cannot be neglected in calculations of ultracold scattering properties based on ab initio potential energies, especially for three-body recombination.

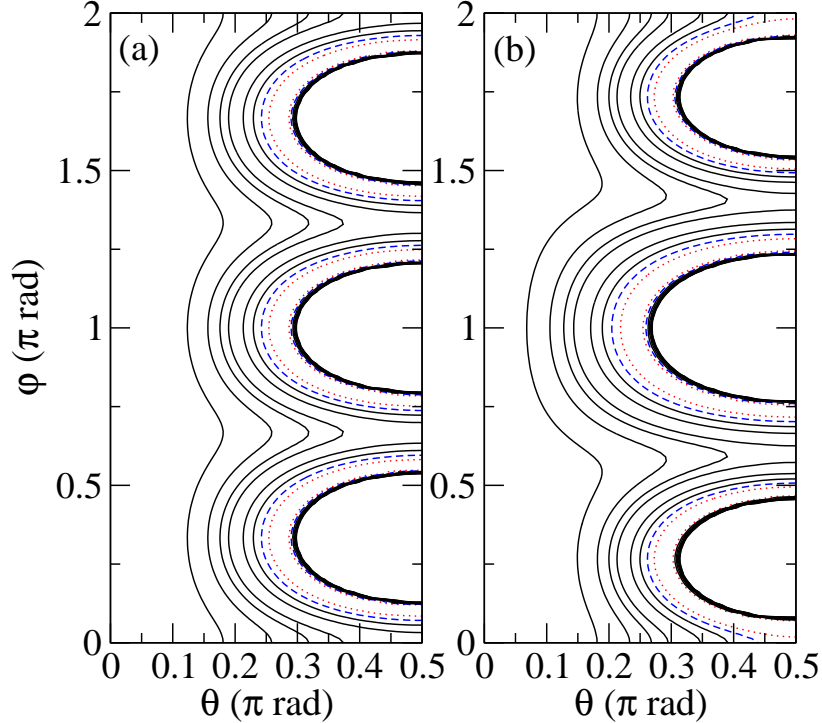


FIG. 1: Contour plot of the potential energy surfaces as functions of the hyperangles θ and φ at $R = 15$ a.u. for a trimer with three identical particles (a) and one with only two identical particles (b). In (a), the translation and reflection symmetries of the potential surface can be seen at $\varphi = n\pi/3$, ($n = 1 - 5$), while in (b) we can identify only the reflection symmetry at $\varphi = \pi$. Exaggerated masses are used in (b) to more easily identify the symmetries. The dotted line corresponds to the lowest contour line, the dashed line to the second lowest contour line.

Acknowledgments

We thank Krzysztof Szalewicz for providing us with codes producing the helium interaction potential used in this work. BDE acknowledges support from the U.S. National Science Foundation and the U.S. Air Force office of Scientific Research.

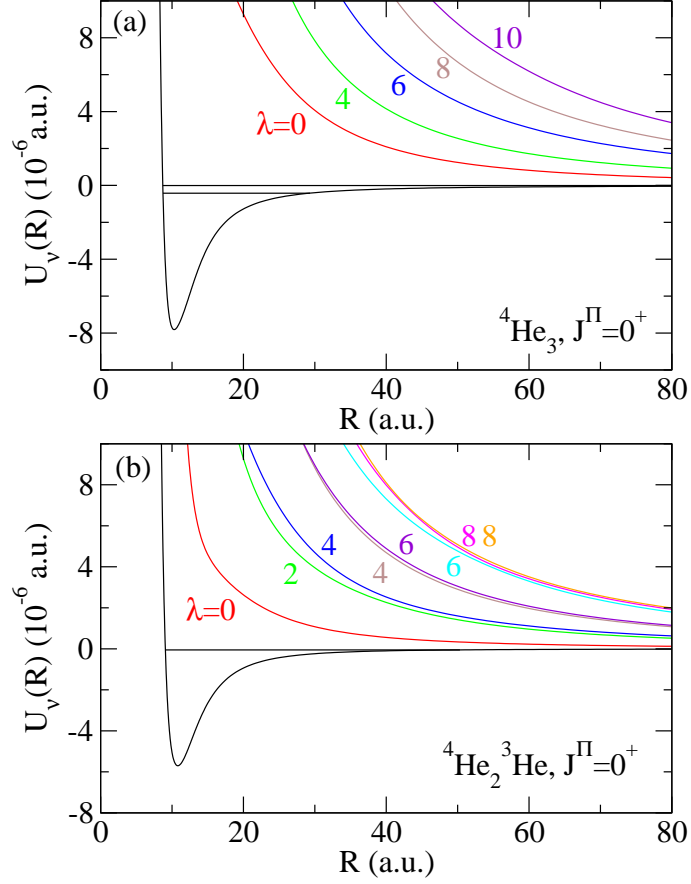


FIG. 2: Adiabatic hyperspherical potential curves $U_\nu(R)$ for (a) ${}^4\text{He}_3$, $J^\Pi = 0^+$ and (b) ${}^4\text{He}_2 {}^3\text{He}$, $J^\Pi = 0^+$. The values of λ indicate the asymptotic behavior of the potential curves, as given in Eq. (22). (a) The 6 lowest potential curves $U_\nu(R)$ for ${}^4\text{He}_3$. In addition, the two bound state energies are shown as horizontal lines. (b) The 9 lowest potential curves $U_\nu(R)$ for ${}^4\text{He}_2 {}^3\text{He}$. The bound state energy is indicated as a horizontal line.

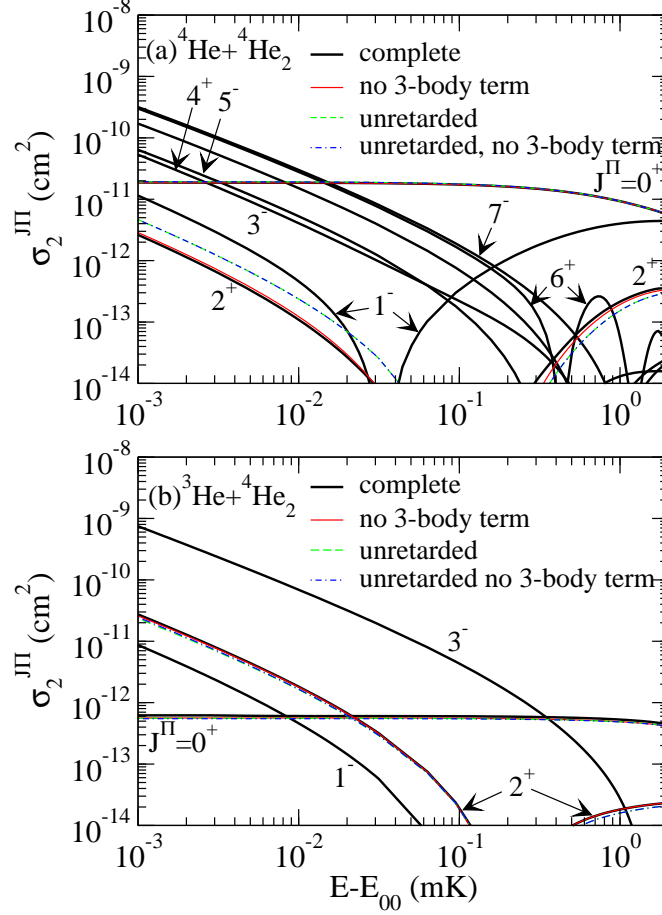


FIG. 3: Partial cross sections $\sigma_2^{J^\Pi}$ for (a) ${}^4\text{He}+{}^4\text{He}_2$ elastic scattering in the $J^\Pi = 0^+, 1^-, \dots, 7^-$ symmetries and for (b) ${}^3\text{He}+{}^4\text{He}_2$ elastic scattering in the $J^\Pi = 0^+, 1^-, 2^+$ and 3^- symmetries, as functions of the collision energy ($E - E_{00}$). The results obtained with the complete helium interaction potential are shown for collision energies $10^{-3} \leq (E - E_{00}) \leq 2$ mK, while those calculated with various combinations of the retarded two-body potential and three-body term are also presented for $J^\Pi = 0^+$ and 2^+ . Note that the three-body breakup threshold is located at $E - E_{00} = 1.564$ mK (with the retarded two-body potential) or 1.728 mK (with the unretarded potential).

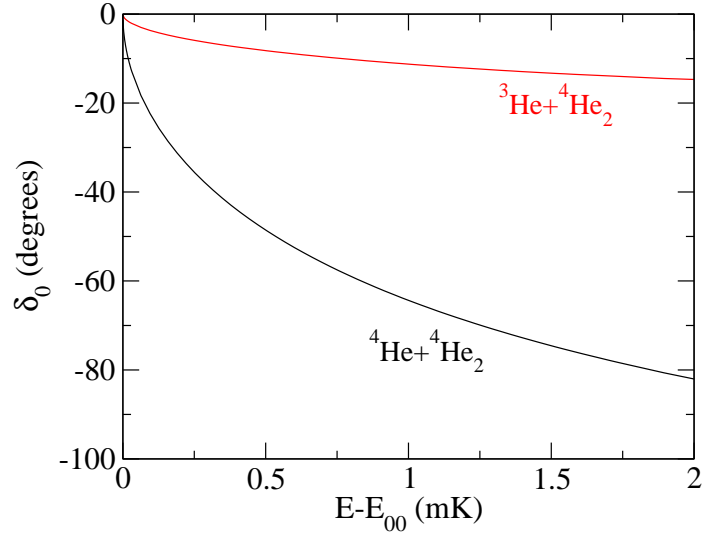


FIG. 4: Phase shifts δ_0 for s -wave atom-dimer scattering as functions of the collision energy. The lower curve shows the results for ${}^4\text{He}+{}^4\text{He}_2$ and the upper one represents the results for ${}^3\text{He}+{}^4\text{He}_2$. Note that the energies are given relative to the two-body dissociation threshold.

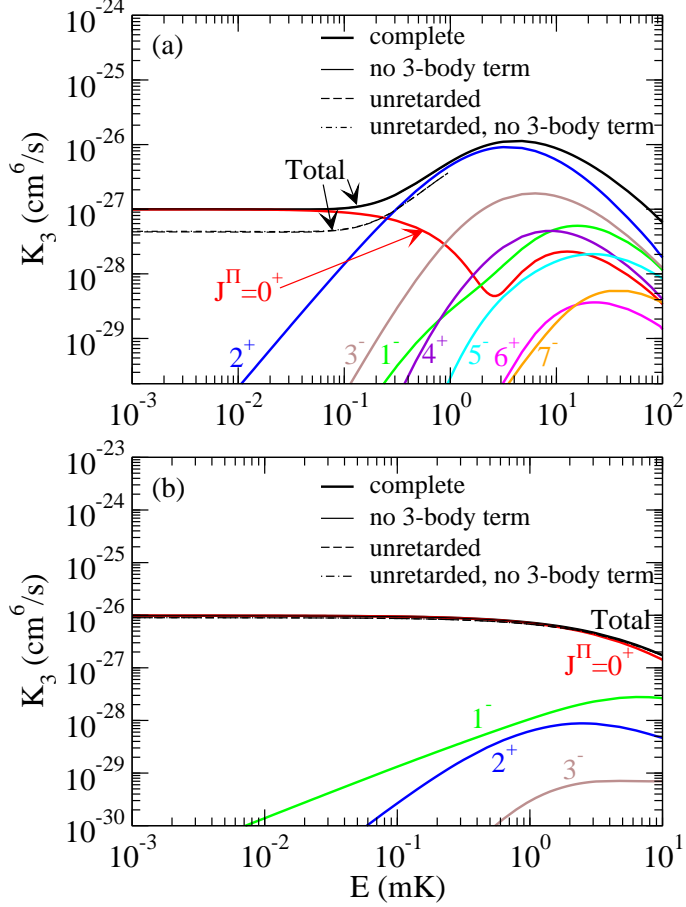


FIG. 5: Total rate K_3 and partial rates $K_3^{J^\Pi}$ for three-body recombination, (a) $^4\text{He}+^4\text{He}+^4\text{He}\rightarrow^4\text{He}_2+^4\text{He}$ and (b) $^4\text{He}+^4\text{He}+^3\text{He}\rightarrow^4\text{He}_2+^3\text{He}$, as functions of the collision energy E . In (a), K_3 and $K_3^{J^\Pi}$ for the $J^\Pi = 0^+, 1^-, 2^+, \dots, 7^-$ symmetries obtained with the complete helium interaction potential are shown while K_3 calculated with all combinations of the retarded two-body potential and three-body term are also presented in the region $E < 1$ mK. In (b), K_3 and $K_3^{J^\Pi}$ for $J^\Pi = 0^+, 1^-, 2^+$ and 3^- symmetries obtained with the complete helium interaction potential are shown along with K_3 calculated with all combinations of the retarded two-body potential and three-body term.

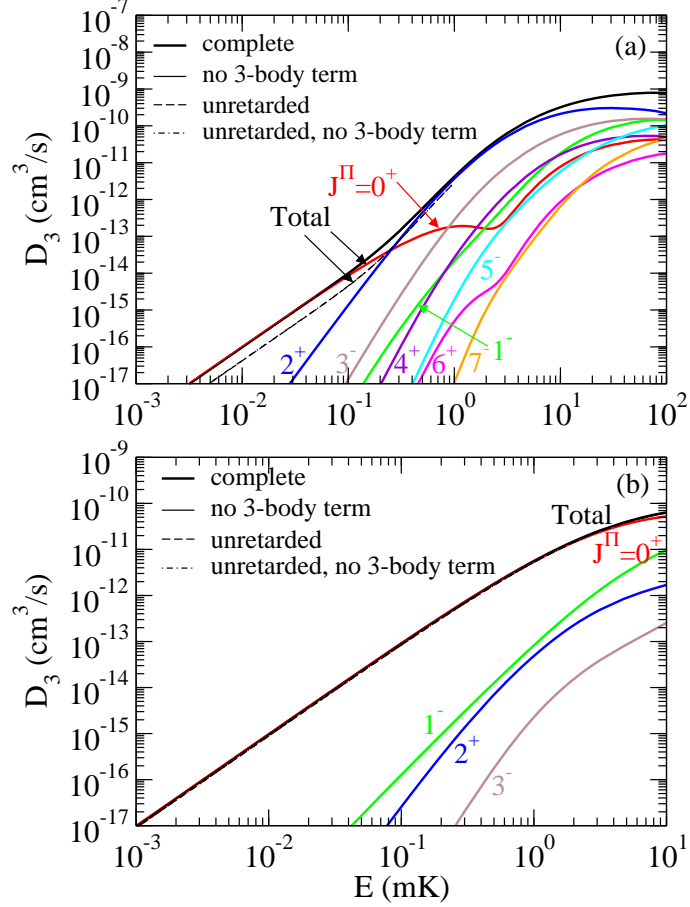


FIG. 6: Total rate D_3 and partial rates $D_3^{J^{\Pi}}$ for collision induced dissociation, (a) ${}^4\text{He}_2 + {}^4\text{He} \rightarrow {}^4\text{He} + {}^4\text{He} + {}^4\text{He}$ and (b) ${}^4\text{He}_2 + {}^3\text{He} \rightarrow {}^4\text{He} + {}^4\text{He} + {}^3\text{He}$, as functions of the collision energy E . In (a), D_3 and $D_3^{J^{\Pi}}$ for the $J^{\Pi} = 0^+, 1^-, 2^+, \dots, 7^-$ symmetries obtained with the complete helium interaction potential are shown while D_3 calculated with all combinations of the retarded two-body potential and three-body term are also presented in the region $E < 1$ mK. In (b), D_3 and $D_3^{J^{\Pi}}$ for the $J^{\Pi} = 0^+, 1^-, 2^+$ and 3^- symmetries obtained with the complete helium interaction potential are shown along with D_3 calculated with all combinations of the retarded two-body potential and three-body term.

TABLE I: $^4\text{He}_2$ bound state energy E_{00} (1 a.u. = 3.1577465×10^8 mK) and scattering length a_{12} calculated with the retarded and unretarded dimer potentials.

potential	E_{00} (a.u.)	E_{00} (mK)	a_{12} (a.u.)	a_{12} (Å)
retarded	-4.953×10^{-9}	-1.564	173.5	91.81
unretarded	-5.472×10^{-9}	-1.728	165.4	87.53

-
- [1] V. Efimov, Phys. Lett. **33B**, 563 (1970).
- [2] V. Efimov, Nucl. Phys. **A210**, 157 (1973).
- [3] V. Efimov, Comm. Nucl. Phys. **19**, 271 (1990).
- [4] T. Kraemer, M. Mark, P. Waldburger, J. G. Danzl, C. Chin, B. Engeser, A. D. Lange, K. Pilch, A. Jaakkola, H.-C. Nägerl, et al., Nature **440**, 315 (2006).
- [5] R. A. Aziz and M. J. Slaman, J. Chem. Phys. **94**, 8047 (1991).
- [6] B. D. Esry, C. D. Lin, and C. H. Greene, Phys. Rev. A **54**, 394 (1996).
- [7] D. Blume, C. H. Greene, and B. D. Esry, J. Chem. Phys. **113**, 2145 (2000).
- [8] E. Nielsen, D. V. Fedorov, and A. S. Jensen, J. Phys. B **31**, 4085 (1998).
- [9] R. Lazauskas and J. Carbonell, Phys. Rev. A **73**, 062717 (2006).
- [10] E. Nielsen and J. H. Macek, Phys. Rev. Lett. **83**, 1566 (1999).
- [11] V. Roudnev, Chem. Phys. Lett. **367**, 95 (2003).
- [12] A. K. Motovilov, W. Sandhas, S. A. Sofianos, and E. A. Kolganova, Eur. Phys. J. D **13**, 33 (2001).
- [13] W. Sandhas, E. A. Kolganova, Y. K. Ho, and M. A. K., Few Body Syst. **34**, 137 (2004).
- [14] R. A. Aziz, A. R. Janzen, and M. R. Moldover, Phys. Rev. Lett. **74**, 1586 (1995).
- [15] H. Suno, B. D. Esry, C. H. Greene, and J. P. Burke, Phys. Rev. A **65**, 042725 (2002).
- [16] J. R. Shepard, Phys. Rev. A **75**, 062713 (2007).
- [17] E. Braaten, H. W. Hammer, D. Kang, and L. Platter (2008), URL <http://www.citebase.org/abstract?id=oai:arXiv.org:0801.1732>.
- [18] M. Jeziorska, W. Cencek, B. Patkowski, B. Jeziorski, and K. Szalewicz, J. Chem. Phys. **127**, 124303 (2007).

TABLE II: Ground and excited state energies for ${}^4\text{He}_3$ and ground state energy for ${}^4\text{He}_2 {}^3\text{He}$ at various levels of approximation. The $\nu_{\text{max}} \rightarrow \infty$ bound state energies are obtained by extrapolation. All energies are given in units of mK, and are relative to the three-body break-up threshold.

		E_0				E_1			
retardation	yes	yes	no	no	yes	yes	no	no	
3-body term	yes	no	yes	no	yes	no	yes	no	
${}^4\text{He}_3$									
BO	-300.86	-301.45	-304.89	-305.48	-3.9277	-3.9315	-4.1839	-4.1879	
adiabatic	-109.78	-109.97	-112.06	-112.26	-2.4175	-2.4189	-2.6047	-2.6061	
$\nu_{\text{max}} = 5$	-129.14	-129.39	-131.70	-131.95	-2.5746	-2.5764	-2.7696	-2.7715	
$\nu_{\text{max}} = 10$	-130.14	-130.39	-132.71	-132.96	-2.5825	-2.5843	-2.7779	-2.7797	
$\nu_{\text{max}} = 15$	-130.44	-130.69	-133.01	-133.27	-2.5848	-2.5866	-2.7803	-2.7821	
$\nu_{\text{max}} = 20$	-130.58	-130.83	-133.15	-133.41	-2.5859	-2.5877	-2.7814	-2.7832	
$\nu_{\text{max}} = 25$	-130.64	-130.89	-133.22	-133.48	-2.5865	-2.5883	-2.7820	-2.7838	
$\nu_{\text{max}} = 30$	-130.68	-130.94	-133.26	-133.52	-2.5868	-2.5886	-2.7824	-2.7842	
$\nu_{\text{max}} = 35$	-130.71	-130.97	-133.28	-133.55	-2.5871	-2.5889	-2.7827	-2.7845	
$\nu_{\text{max}} \rightarrow \infty$	-130.86	-131.12	-133.44	-133.70	-2.5882	-2.5900	-2.7838	-2.7856	
${}^4\text{He}_2 {}^3\text{He}$									
BO	-90.700	-90.945	-93.201	-93.454					
adiabatic	-11.088	-11.125	-11.985	-12.024					
$\nu_{\text{max}} = 5$	-14.921	-14.973	-15.982	-16.038					
$\nu_{\text{max}} = 10$	-15.432	-15.486	-16.514	-16.572					
$\nu_{\text{max}} = 15$	-15.644	-15.699	-16.734	-16.792					
$\nu_{\text{max}} = 20$	-15.735	-15.790	-16.828	-16.887					
$\nu_{\text{max}} = 25$	-15.818	-15.873	-16.914	-16.973					
$\nu_{\text{max}} = 30$	-15.863	-15.918	-16.960	-17.019					
$\nu_{\text{max}} = 35$	-15.898	-15.953	-16.996	-17.055					
$\nu_{\text{max}} \rightarrow \infty$	-16.237	-16.293	-17.346	-17.405					

- [19] W. Cencek, M. Jeziorska, O. Akin-Ojo, and K. Szalewicz, *J. Phys. Chem.* **111**, 11311 (2007).
- [20] P. Barletta and A. Kievsky, *Phys. Rev. A* **64**, 042514 (2001).
- [21] F. Luo, G. McBane, G. Kim, C. F. Giese, and W. R. Gentry, *J. Chem. Phys.* **98**, 3564 (1993).
- [22] F. Luo, C. F. Giese, and W. R. Gentry, *J. Chem. Phys.* **104**, 1151 (1996).
- [23] W. Schöllkopf and J. Toennies, *Science* **266**, 1345 (1994).
- [24] W. Schöllkopf and J. Toennies, *J. Chem. Phys.* **104**, 1155 (1996).
- [25] T. G. Lee, B. D. Esry, B.-C. Gou, and C. D. Lin, *J. Phys. B* **34**, L203 (2001).
- [26] E. A. Kolganova, A. K. Motovilov, and W. Sandhas, *Nucl. Phys. A* **790**, 752 (2007).
- [27] K. Szalewicz, private communication (2008).
- [28] C. D. Lin, *Phys. Rep.* **257**, 1 (1995).
- [29] B. R. Johnson, *J. Chem. Phys.* **73**, 5051 (1980).
- [30] B. K. Kendrick, R. T. Pack, R. B. Walker, and E. F. Hayes, *J. Chem. Phys.* **110**, 6673 (1999).
- [31] M. Aymar, C. H. Greene, and E. Luc-Koenig, *Rev. Mod. Phys.* **68**, 1015 (1996).
- [32] R. C. Whitten and F. T. Smith, *J. Math. Phys.* **9**, 1103 (1968).
- [33] B. Lepetit, Z. Peng, and A. Kuppermann, *Chem. Phys. Lett.* **166**, 572 (1990).
- [34] L. M. Delves, *Nucl. Phys.* **9**, 391 (1958).
- [35] L. M. Delves, *Nucl. Phys.* **20**, 275 (1960).
- [36] C. de Boor, *A Practical Guide to Splines* (Springer, New York, 1978).
- [37] M. Salci, E. Yarevsky, S. B. Levin, and N. Elander, *Int. J. Q. Chem.* **107**, 464 (2007).
- [38] D. Bressanini, M. Zavaglia, M. Mella, and G. Morosi, *J. Chem. Phys.* **112**, 717 (2000).
- [39] H. Suno, B. D. Esry, and C. H. Greene, *Phys. Rev. Lett.* **90**, 053202 (2003).
- [40] J. P. Burke, Jr., Ph.D. thesis, University of Colorado (1999).
- [41] B. D. Esry, C. H. Greene, and H. Suno, *Phys. Rev. A* **65**, 010705 (2001).
- [42] P. Soldán, M. T. Cvitaš, J. M. Hutson, P. Honvault, and J.-M. Launay, *Phys. Rev. Lett.* **89**, 153201 (2002).
- [43] M. T. Cvitaš, P. Soldán, J. M. Hutson, P. Honvault, and J.-M. Launay, *Phys. Rev. Lett.* **94**, 033201 (2005).